Carrier Power to Intermodulation-Distortion Power-Ratio-Increasing Technique in Active Phased-Array Antenna Systems

Takana Kaho, Tadao Nakagawa, *Member, IEEE*, Katsuhiko Araki, and Kohji Horikawa, *Member, IEEE*

***Abstract*—This paper describes a novel technique to compensate for the intermodulation (IM) distortion components of high-power amplifiers in an active phased-array antenna system. This technique uses IM phase control to break the strong association between carriers and IM components, and can make the radiation patterns of carriers and IM components different on active phased-array antenna systems. As a result, carrier power to IM power ratio (C/IM) is increased in the carrier-beam direction. A newly developed IM controller can increase the C/IM of near-saturated solid-state power amplifiers and, therefore, achieve high power efficiency. This paper shows experimental results confirming this technique using a six-element linear array.**

***Index Terms*—Intermodulation (IM) distortion, monolithic microwave integrated circuits (MMICs), phased array, power amplifiers, satellite communication on-board systems.**

I. Introduction

In MOBILE satellite communication systems, there is a demand for increased capacity due to the advent of broad-band communication services to supply voice communication, E-mail, World Wide Web content, movies, etc. However, if mobile satellite communication systems are to support smaller earth stations, such as handy phones, the satellites must have high levels of effective isotropic radiated power (EIRP). One of the most interesting approaches to achieve high EIRP is an active phased-array antenna system [1]. Such a system requires high-power amplifiers that can offer kilowatt-class RF power. Since mobile satellite communication systems use multicarrier transmission, high carrier power to intermodulation (C/IM) power ratios is required. However, amplifiers must tradeoff power efficiency against intermodulation (IM) distortion components. Thus, on-board high-power amplifiers must be used at low power efficiency to minimize IM components. This is a serious problem because satellites have poor heat dissipation. Many compensation techniques have been developed that try to reduce the nonlinear distortion of a high-power amplifier. Predistortion linearizers have been used for satellite high-power amplifiers because of their simplicity, light weight, and low power consumption [2], [3]. Future active phased-array antenna system will have hundred of elements composed of high-power amplifiers and antennas to achieve high-frequency efficiency. The monolithic-microwave integrated-circuit (MMIC) technique can make numerous circuits of the same quality and is suited to producing the predistortion linearizer for an active phased-array antenna system. However, conventional predistortion linearizers operate poorly in the near-saturated region, which offers high power efficiency. It is important to realize distortion compensation techniques that allow high-power amplifiers to operate in the near-saturated region.

To address this problem, we proposed an IM controller that can control the IM of a near-saturated high-power amplifier, and an IM control technique for use with a balanced high-power amplifier array [4]–[6]. This paper describes an IM control technique in an active phased-array antenna system. The principle of the technique is described as well as the developed IM controller. The experimental results obtained by applying IM control to a six-element linear array antenna are reported. It was tested to create an IM radiation pattern that is different from a carrier radiation pattern.

II. IM Control Technique

We call our proposed technique the IM control technique. It controls IM phase in an active phased-array antenna system. Fig. 1 shows the concept of the IM control technique. In a conventional active phased-array antenna system, when carriers are combined in-phase, the IM components are also combined in-phase because of the strong association between carriers and IM components. Accordingly, carrier-beam direction and IM beam direction are almost the same, as shown in Fig. 1(a). On the other hand, in the proposed active phased-array antenna system, when carriers are combined in-phase, the IM components are not combined in-phase due to the IM controllers. Hence, the carrier radiation pattern and IM radiation pattern are different, as shown in Fig. 1(b). As a result, C/IM is increased along the carrier-beam direction.

A. Principle of IM Controller

To improve C/IM, each IM component in a high-power amplifier must be controlled. The required functions for the IM controller are IM phase control and amplitude control. To realize the proposed IM control technique, we selected a predistortion-type linearizer in the RF frequency band to control the

Manuscript received April 4, 2002; revised August 27, 2002. This work was supported in part by the NTT Network Innovation Laboratories, NTT Corporation.

T. Kaho, T. Nakagawa, and K. Araki are with the NTT Network Innovation Laboratories, NTT Corporation, Yokosuka 239-0847, Japan (e-mail: kaho@ wslab.ntt.co.jp).

K. Horikawa is with the Radio Network Development Department, NTT DoCoMo Inc., Yokosuka 234-8536, Japan.

Digital Object Identifier 10.1109/TMTT.2002.805136

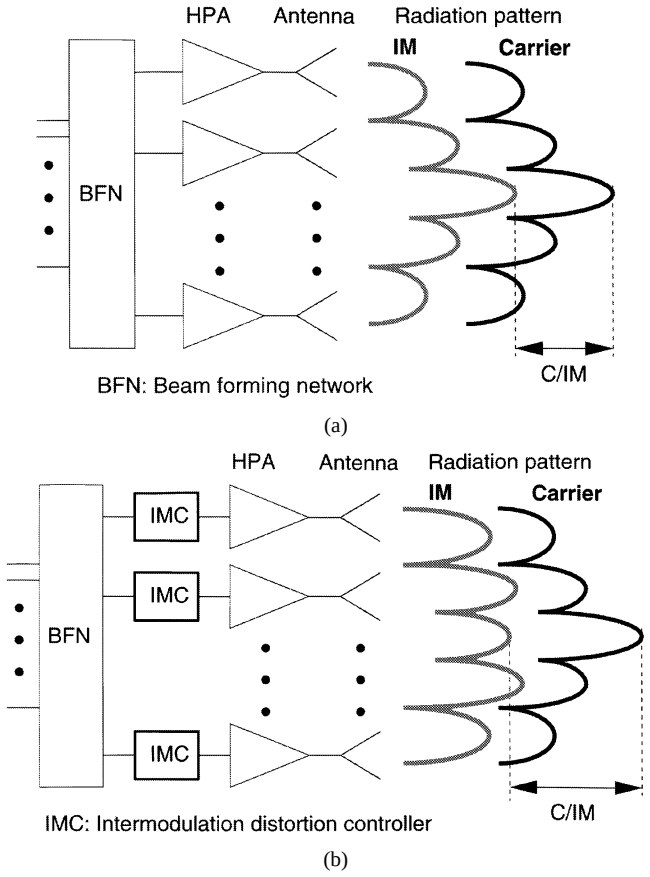

Fig. 1. Concept of the IM control technique in active phased-array antenna system. (a) Conventional active phased-array antenna system. (b) Proposed active phased-array antenna system.

IM phase. It is suitable for an on-board high-power amplifier because it is simple, light weight, and has low power consumption. We proposed an even-order distortion implemented IM distortion controller (EODIC). It has been evaluated as a linearizer [7], and shown to offer high IM control performance [8].

The block diagram and functions of the EODIC for a two-tone carrier input are shown in Fig. 2. The EODIC consists of a two-way power divider, a variable phase shifter (VPS) (see Fig. 2), a frequency doubler, two variable-gain amplifiers (i.e., VGA1 and VGA2 in Fig. 2), an amplitude modulator, and an output buffer amplifier. Since the spectra are converted to the second harmonic frequency band ($2\omega_0$) in the nonlinear path, the residual carriers in the fundamental frequency band are removed. The EODIC controls the phase of IM in $2\omega_0$ by a VPS, which minimizes the effect on the carriers in the linear path. This makes the EODIC a suitable tool for implementing the IM control technique.

The principle of the EODIC has already been explained mathematically in [6]. This paper presents a brief description. When two-tone carriers having frequencies ω_1 and ω_2 are input to the EODIC, the input carriers $C_{2\text{tone}}$ are described as

$$C_{2\text{tone}} = A\sin(\omega_1 t + \phi_1) + A\sin(\omega_2 t + \phi_2) \tag{1}$$

where A is the amplitude of each carrier and ϕ_1 and ϕ_2 are the initial phases of the respective carriers. The input carriers are divided among the linear and nonlinear paths. In the nonlinear path, carrier phase is shifted by the VPS, while carrier amplitude is controlled by the VGA1. The carriers in the nonlinear path are then converted into second-order harmonics $\text{IM}_{2\text{nd}f}$ by the frequency doubler as follows:

$$\text{IM}_{2\text{nd}f} = \alpha A'^2 \Big\{ \sin\left(\omega_1 t + \phi_{21} + \Delta\phi_1^{\text{VPS}}\right) + \sin\left(\omega_2 t + \phi_{22} + \Delta\phi_2^{\text{VPS}}\right) \Big\}^2 \tag{2}$$

where α is the conversion factor of the frequency doubler, A' is the amplitude of each carrier, and ϕ_{21} and ϕ_{22} are the phases of the respective signals at the output point of the frequency doubler; they depend on the electrical length of the path. Equation (2) contains dc, the mixing products in the low-frequency band, and the mixing products in the second-order harmonic frequency band. The dc and mixing product in the low-frequency band are filtered out by VGA2. Additionally, VGA2 can control the amplitude of $\text{IM}_{2\text{nd}f}$ by using VGA2 control voltage V_2. Thus, $\text{IM}_{2\text{nd}f}$ is expressed as $\text{IM}'_{2\text{nd}f}$ as follows:

$$\begin{aligned}\text{IM}'_{2\text{nd}f} =& A'' \Big\{ \cos\left(2\omega_1 t + 2\phi_{21} + 2\Delta\phi_1^{\text{VPS}}\right) \\ &+ \cos\left(2\omega_2 t + 2\phi_{22} + 2\Delta\phi_2^{\text{VPS}}\right) \\ &+ 2\cos\Big((\omega_1 + \omega_2)t + \phi_{21} + \phi_{22} \\ &+ \Delta\phi_1^{\text{VPS}} + \Delta\phi_2^{\text{VPS}}\Big)\Big\}. \end{aligned} \tag{3}$$

In practice, input signal leakage is contained in the output spectra of the frequency doubler. However, this component is also filtered out.

The amplitude modulator causes IM components to be generated in the fundamental frequency band

$$\begin{aligned}\text{AM}_{\text{out}} =& C_{l\text{in}}(K + \beta \cdot \text{IM}'_{2\text{nd}f}) \\ =& K \cdot C_{l\text{in}} + \beta \cdot C_{l\text{in}} \cdot \text{IM}'_{2\text{nd}f} \end{aligned} \tag{4}$$

where AM_{out} is the output of the amplitude modulator, $C_{l\text{in}}$ is the input carriers of amplitude modulator via the linear path, K is a factor of $C_{l\text{in}}$, which indicates the insertion loss for the input carriers $C_{l\text{in}}$, β is a modulation factor that depends on the amplitudes and phases of $C_{l\text{in}}$ and $\text{IM}'_{2\text{nd}f}$ and on the characteristics of the amplitude modulator, such as bias voltages. Here, AM_{out} consists of two terms. The first term indicates the characteristics of the carriers, while the second term indicates those of the odd-order distortion component. The third-order distortion components in the fundamental frequency band of the second term $\text{IM3}_{\text{fund}f}$ are given as follows:

$$\begin{aligned}\text{IM3}_{\text{fund}f} =& A''' \Big\{ 3\sin\left(\omega_1 t + \phi_{31} + 2\Delta\phi^{\text{VPS}}\right) \\ &+ 3\sin\left(\omega_2 t + \phi_{32} + 2\Delta\phi^{\text{VPS}}\right) \\ &+ \sin\Big((2\omega_1 - \omega_2)t + \phi_{33} + 2\Delta\phi^{\text{VPS}}\Big) \\ &+ \sin\Big((2\omega_2 - \omega_1)t + \phi_{34} + 2\Delta\phi^{\text{VPS}}\Big)\Big\}. \end{aligned} \tag{5}$$

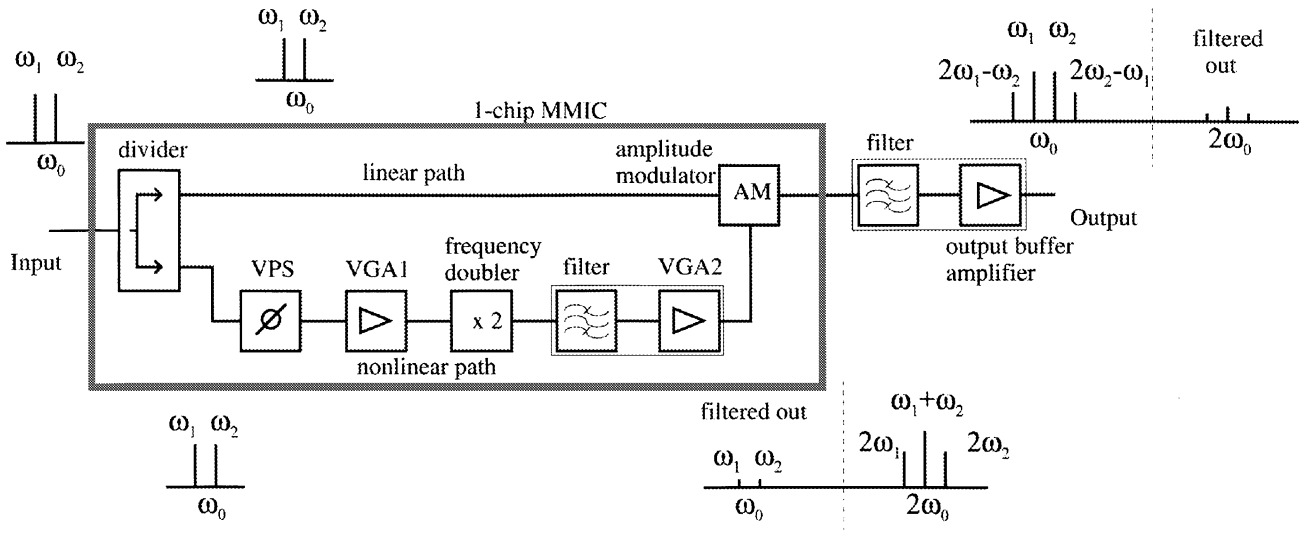

Fig. 2. Block diagram of the developed IM controller EODIC.

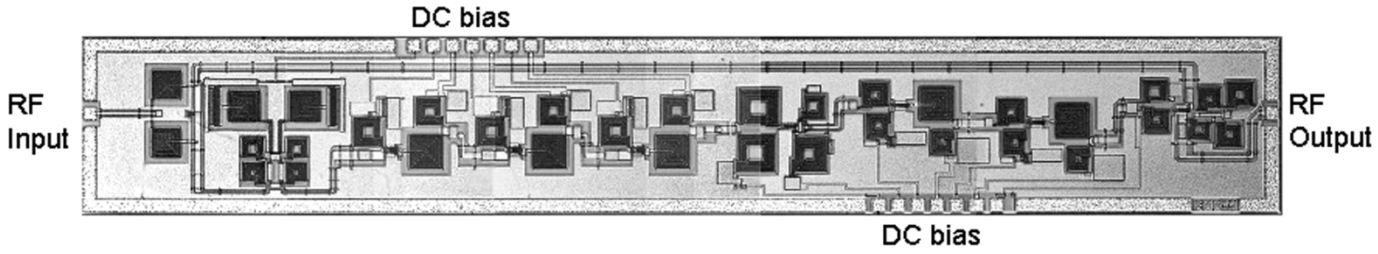

Fig. 3. Microphotograph of an EODIC. The chip size is 1.4 × 9.2 mm, and power consumption is approximately 300 mW.

The amplitude of $\mathrm{IM3}_{\mathrm{fund}f}$, A''' can be controlled by the bias voltages of VGA1 and VGA2, the frequency doubler, and the amplitude modulator in the EODIC. $\phi_{3m}(1 \leq m \leq 4)$, which indicates signal phase, depends on the electrical lengths of the divider, linear path, nonlinear path and amplitude modulator and, thus, cannot be controlled by the VPS. The wireless communication system considered here is narrow-band and, in this case, it can be assumed for the phase shift that $\Delta\phi_1^{\mathrm{VPS}} \cong \Delta\phi_2^{\mathrm{VPS}}$. This assumed $\Delta\phi_1^{\mathrm{VPS}} = \Delta\phi_2^{\mathrm{VPS}} = \Delta\phi^{\mathrm{VPS}}$ and also that $\phi_{33} \cong \phi_{31}$ and $\phi_{34} \cong \phi_{32}$.

Therefore, when the VPS can control the phase from 0° to 180°, the phase of $\mathrm{IM3}_{\mathrm{fund}f}$ can be controlled from 0° to 360°.

In conventional linearizers, carriers in the linear path are affected by the carrier leakage from the nonlinear path. In the EODIC, carrier leakage can be filtered out. However, there are mixing products at the same frequencies as the carriers [first and second terms in (5)]. Since this has a much smaller impact than carrier leakage, the EODIC offers superior distortion control performance.

B. Developed IM Controller MMIC

We developed an EODIC on a GaAs chip. Fig. 3 shows the microphotograph of the EODIC. The chip size is 1.4 × 9.2 mm and the power consumption is approximately 300 mW. The EODIC was redesigned to control IMs of a near-saturated high-power amplifier. The performance of the previous EODIC was inadequate for producing sufficient IMs [8]. In the previous EODIC, the input power of the amplitude modulator should be large. When the input power of the EODIC was increased to generate sufficient IMs, the EODIC's VPS generated unnecessary and uncontrollable IMs when the input power was large, and the EODICs output buffer amplifier was saturated. Therefore, the previous EODIC could not control the saturated high-power amplifier. The new EODIC MMIC has three-stage amplifiers such as VGA1 to increase the gain, and does not have an output buffer amplifier. This change allows the new EODIC to control the IMs of a near-saturated high-power amplifier.

Fig. 4 shows the measured phase control performance of a near-saturated high-power amplifier with the EODIC. The third-order intermodulation (IM3) phase could be controlled through 350° by using the VPS. The carrier phase varied about ±27° by the VPS control voltage. This can be explained by the fact that the amplitude of an IM whose frequency is the same as the carrier [first and second terms in (5) cannot be negligible in the near-saturated region. The measured result of the carrier indicated that it is a combined vector of the carrier and the generated IM component at the same frequency, see Fig. 4(c)]. However, in actual situation, the effect of the IM may be small to the carrier because the power level is smaller than the carrier's level.

III. Experimental Results

A. Experimental Setup of the Linear Array

The proposed IM control technique was demonstrated experimentally using a six-element linear array comprising 10-W class

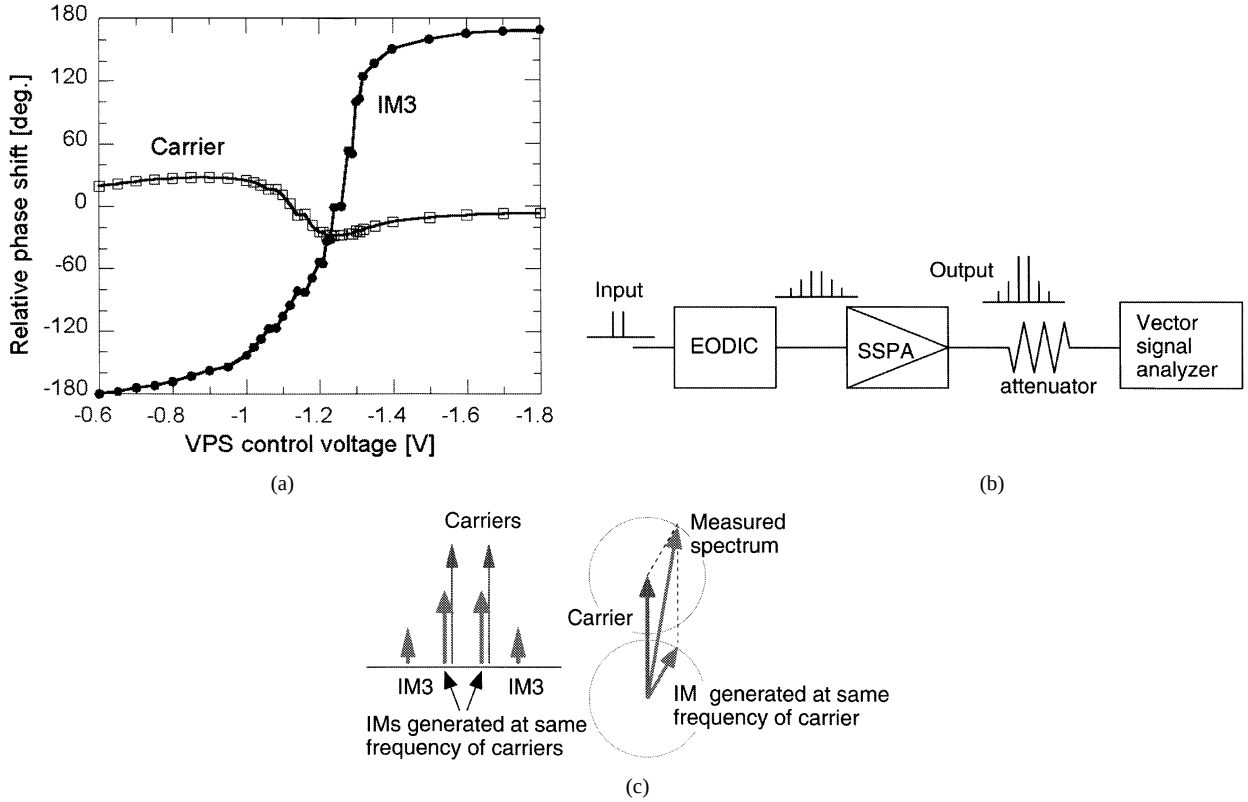

Fig. 4. IM phase control performance of an EODIC. (a) Measured IM phase control performance of an EODIC. (b) Experimental setup. (c) Explanation for carrier phase deviation.

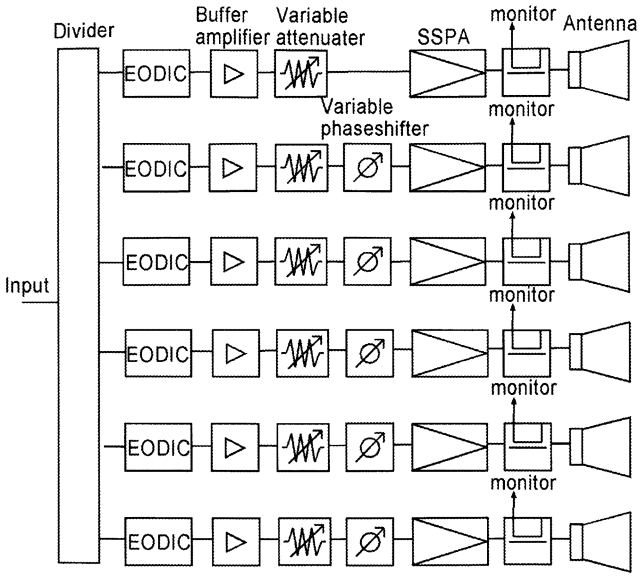

Fig. 5. Block diagram of six-element linear array.

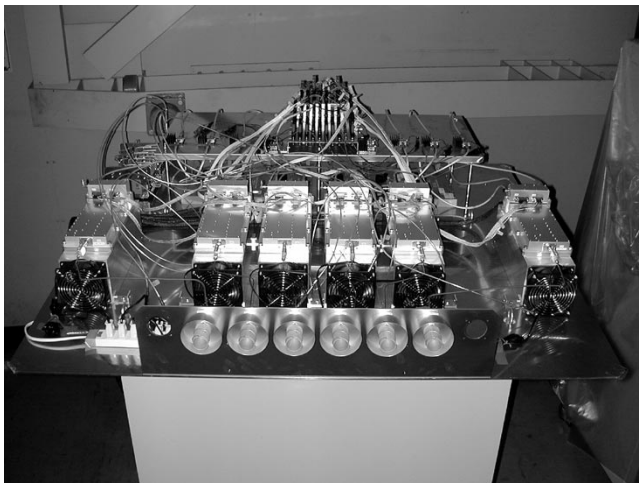

Fig. 6. Photograph of the six-element linear array.

solid-state power amplifiers (SSPAs) in the S-band. The experimental block diagram is shown in Fig. 5. In this linear array, one EODIC was placed in front of each SSPA. The phase shifter, buffer amplifier, and attenuator were used to equalize electrical length and loss. A 20-dB directional coupler was located between each SSPA and the transmitting antenna to monitor the output spectra. Helical antennas were used as the transmitting antennas. The antennas were regularly spaced at intervals of 0.8 λ (in 2.5 GHz). Fig. 6 shows a photograph of the six-element linear array.

Fig. 7 shows the experimental setup of the six-element linear array. The linear array was set on a turntable in a radio anechoic chamber. The transmitting antenna was the same type as the receiving antenna. Carrier and IM receiving power were monitored using a spectrum analyzer. The distance from the front of the six-element linear antenna to the receiving antenna was approximately 6 m for far-field measurement. Radiation patterns were measured from -90° to 90° in azimuth by driving the turntable.

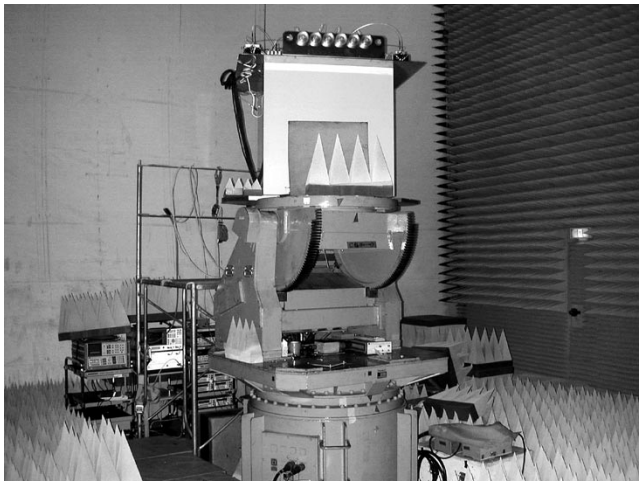

(a)

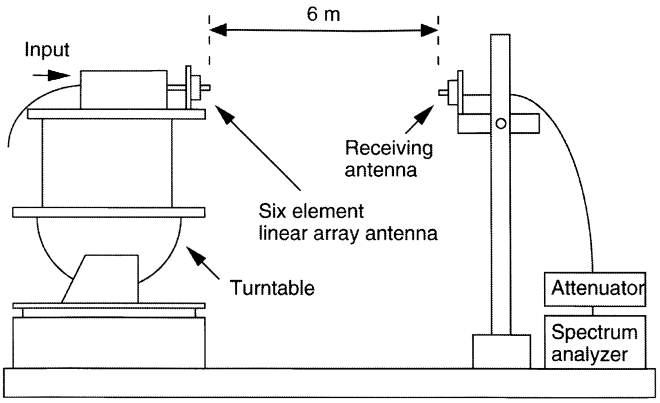

(b)

Fig. 7. Far-field experiment in a radio anechoic chamber. (a) Active phased array on the turntable. (b) Experimental setup for far-field measurement.

TABLE I
MEASURED FREQUENCY OF CARRIERS AND IM COMPONENTS

	Lower side frequency	Upper side frequency
Carrier	2.517 GHz	2.518 GHz
IM3	2.516 GHz	2.519 GHz
IM5	2.515 GHz	2.520 GHz
IM7	2.514 GHz	2.521 GHz

B. Far-Field Measurement

In this experiment, two-tone carriers were used to measure the radiation pattern of the carriers, IM3s, fifth-order intermodulations (IM5s), and seventh-order intermodulations (IM7s). The measured carrier frequencies and IM components' frequency are shown in Table I.

Fig. 8 shows the measured radiation pattern of "Without EODIC" for the carrier and IM3 [see Fig. 8(a)] and IM5 and IM7 [see Fig. 8(b)]. The vertical axis is the receiving power relative to the carrier receiving power without EODIC at 0° in azimuth. The data shown in this figure were summations of the receiving powers in the lower and upper side frequency bands (see Table I). The carrier amplitude and phase were adjusted to be uniform in front of the transmitting antennas. Since the

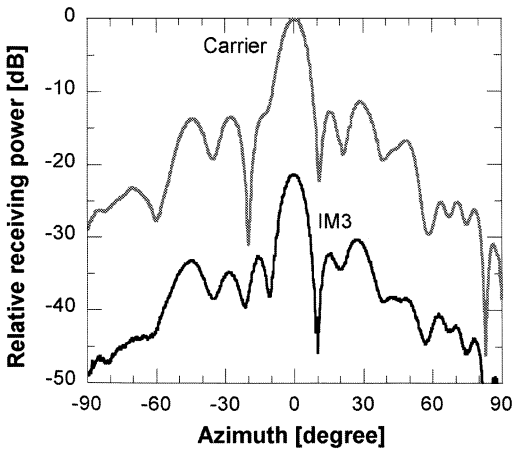

(a)

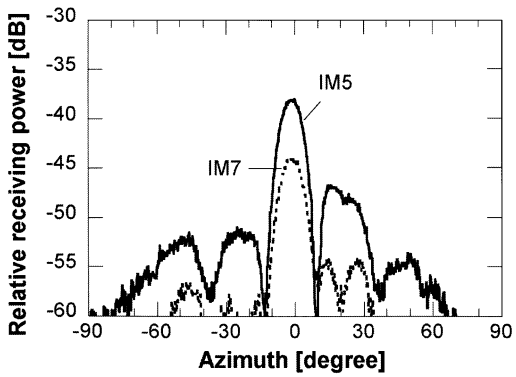

(b)

Fig. 8. Measured radiation pattern without an EODIC. (a) Carrier and IM3. (b) IM5 and IM7.

drain voltages of the EODIC's frequency doublers were set as 0 V, the EODICs did not generate IM components. We then treated the condition as "Without EODIC." We measured the radiation patterns at approximately a 1-dB gain compression point (P1 decibel) that had a 21-dB C/IM ratio.

Fig. 9 shows the measured radiation patterns with an EODIC for the carrier and IM3 [see Fig. 9(a)] and IM5 and IM7 [see Fig. 9(b)]. The bias voltages of the VPS, VGA1, and amplitude modulator were adjusted manually by monitoring the output spectra with a vector signal analyzer. The EODICs were controlled so that C/IM3 was more than 21 dB at the carrier 3-dB beamwidth. First, the bias voltage of each EODIC's amplitude modulator was adjusted to control the IM3 components. Also, the bias voltages of EODICs' phase shifters were adjusted to randomize the IM3 phases. The carrier input power level was adjusted so that the carrier receiving power was the same as those without an EODIC.

In Fig. 8, without an EODIC, the carrier-beam direction and IM3 beam directions were 0° in azimuth. The IM5 and IM7 beam direction were 0°. Their radiation patterns showed a remarkable degree of correspondence and evidence of the strong association between the carrier and IM components.

On the other hand, with EODIC carrier-beam direction was 0°, but the IM3 components were distributed as shown in Fig. 9. There were three beams at $-37°$, 3°, and $+33°$. The IM5 radiation pattern was also distributed. It was similar to that of the IM3

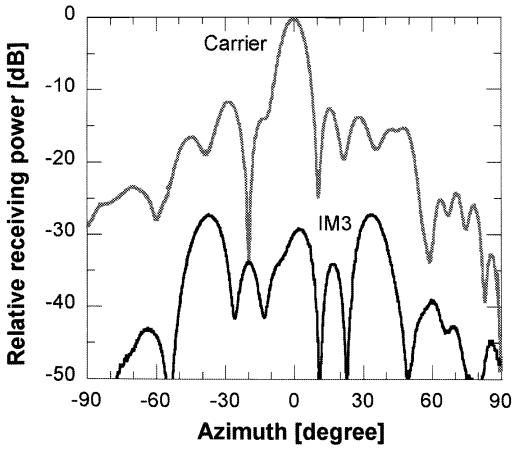

(a)

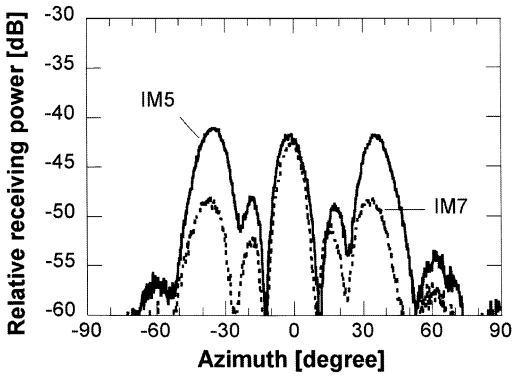

(b)

Fig. 9. Measured radiation pattern with an EODIC. (a) Carrier and IM3. (b) IM5 and IM7.

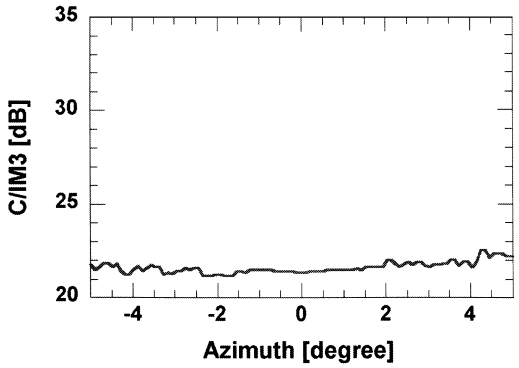

(a)

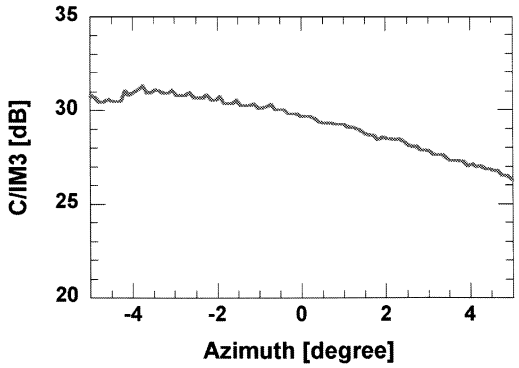

(b)

Fig. 10. Measured C/IM3: (a) without an EODIC and (b) with an EODIC.

component. The radiation patterns of the IM3 and IM5 looked different from that of the carrier. The distribution effect of the IM7 radiation pattern was smaller than those of the IM3 and IM5 components.

By comparing without and with an EODIC, both carriers had similar radiation patterns with the same receiving power in the carrier-beam direction. However, the IM radiation patterns were different. With an EODIC, the IM3 and IM5 receiving power were less than those without an EODIC for the carrier-beam direction. However, IM7 receiving power was higher than those without an EODIC for the carrier-beam direction. It is supposed that the frequency characteristic of the EODIC was different from that of the SSPA.

Fig. 10 shows the C/IM3 ratio versus azimuth in -5°–5°. Fig. 10(a) shows those without an EODIC, and Fig. 10(b) shows those with an EODIC. The carrier receiving power and IM3 receiving power were used the summation of the two components in the lower and upper side frequency bands. In Fig. 10(a), the C/IM3 ratio was an almost constant value of approximately 21 dB in -5°–5°. On the other hand, with an EODIC, the C/IM3 ratio was from 26 to 31 dB, as shown in Fig. 10(b). By comparing these figures, within the 3-dB beamwidth of the carrier beam (-4.3°–4.3°), the C/IM3 ratio with the EODIC was 5–10 dB higher than that obtained without an EODIC. C/IM3 was improved by 5 dB from 21 to 26 dB along the carrier-beam direction.

We measured carrier and IM3 receiving power versus carrier input power for the carrier 3-dB beamwidth. We adjusted the EODIC to minimize the IM3s receiving power at a near-saturated region of an SSPA. The bias voltages of the EODIC's VPS, VGA1, and amplitude modulator were adjusted manually. The bias voltages were then fixed during the measurement.

In Figs. 11–13, the carrier and IM3 data used the averages of the two carriers and two IM3 components, respectively. The narrow dashed lines and solid lines indicate the cases without and with an EODIC, respectively. The input power levels were different with and without an EODIC because the EODIC has insertion loss that depends on bias voltages. We then used the input backoff (IBO) level to compare the performance. The IBO shows the amount of backoff level from the input power that saturates the amplifier. The low IBO level shows the high input power and near-saturated region of an amplifier. In the case without an EODIC, we defined the saturate power as the 2-dB gain compression point (P2 decibel point) when two-tone carriers are input to the SSPAs. In the case with an EODIC, we defined 0 dB of the IBO level as the input power that could achieve the same carrier receiving power of the saturate power without an EODIC.

Fig. 11 shows the measured carrier and IM3 receiving power versus the IBO level. It used the maximum power level within the carrier 3-dB beamwidth. In Fig. 11, with an EODIC, the carrier was linearized at a low IBO level, then the 0-dB IBO level was a P1 decibel point. Without an EODIC, the carrier was decreased gradually at low IBO level. At the 5-dB IBO level, the decrease was 0.5 dB, at the 2.5-dB IBO level it was a P1 decibel point, and at the 0-dB IBO level, it was a P2 decibel point. With

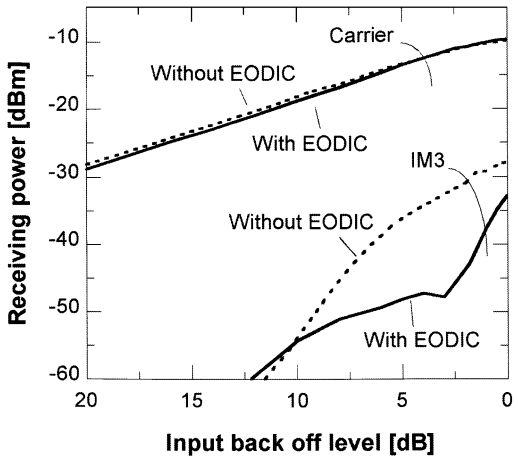

Fig. 11. Measured carrier and IM3 receiving power versus IBO level.

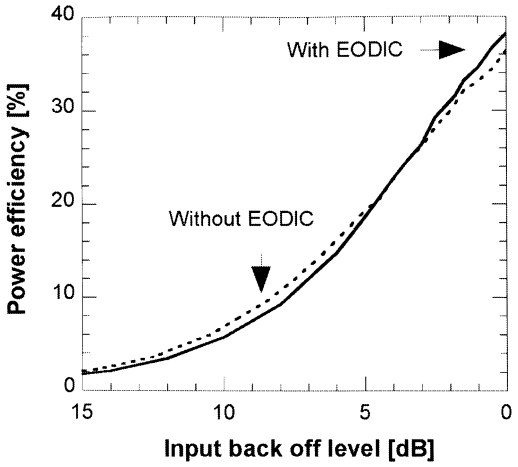

Fig. 12. Power efficiency versus IBO level.

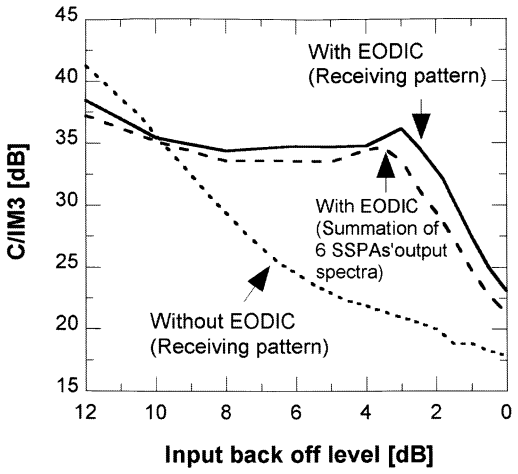

Fig. 13. Measured C/IM3 versus IBO level.

an EODIC, the IM3 receiving power was less than that without an EODIC from 11 to 0 dB of the IBO level.

Fig. 12 shows the total power efficiency versus IBO level of the SSPA with and without an EODIC. The EODIC's power consumption was considered in the data with an EODIC. Approaching the saturate power, both of the power efficiencies were increased. They showed almost the same character.

Fig. 13 shows the measured C/IM3 ratio versus IBO level at a 3-dB beamwidth of the carrier beam. It used the minimum C/IM3 level within the carrier 3-dB beamwidth. In Fig. 13, a wide dashed line indicates the case of the SSPAs with an EODIC that was the ratio between the total amount of the carrier power and that of the IM3 power of the six SSPAs. The ratio is equivalent to the C/IM3 that is obtained when both carriers and IM3s of the six SSPAs are combined in-phase. The amplitude of the carriers and the IMs of the six SSPAs' output were monitored by a vector signal analyzer via the directional couplers located between the SSPA output and helical antenna (see Fig. 5). In Fig. 13, the C/IM3 ratio of the SSPA with an EODIC (solid line) was higher than that of the summation of the six SSPAs' output spectra (wide dashed line). Namely, the C/IM3 in the carrier-beam direction was higher than that of the summation of six SSPAs' output spectra that were monitored via the directional couplers. This result shows the distribution effect of the proposed IM control technique. The C/IM3 ratio was increased 3.5 dB at the 2-dB IBO level. It is supposed that the distribution effect will be large when the number of elements become large. At the 0.8-dB IBO level, the C/IM3 ratio with an EODIC was 8 dB higher than that without an EODIC, i.e., from 18 to 26 dB.

To achieve a C/IM3 ratio by more than 26 dB, the SSPAs without an EODIC have a low power-added efficiency of approximately 14%. By using an EODIC, the SSPAs have a power-added efficiency of approximately 36%. Therefore, the result shows that the power-added efficiency is increased from approximately 14% to 36% to achieve a C/IM3 ratio of 26 dB.

IV. Conclusion

A novel technique to improve the C/IM distortion power ratio has been tested. Its effectiveness has been demonstrated in an experiment using a six-element linear array antenna with EODICs. By using EODICs, the measured IM3, IM5, and IM7 distortion radiation patterns could be different from those of the case without an EODIC. The carrier radiation pattern was almost the same shape as that of the case without an EODIC. We also confirmed the good input to output performance to achieve high C/IM3, and confirmed the EODIC's IM reduction performance and IM distribution effect. By using an EODIC and the IM control technique, the C/IM3 was improved by 8 dB, from 18 to 26 dB along the carrier-beam direction. To achieve a C/IM3 ratio of over 26 dB, the power-added efficiency was increased from approximately 14% to 36%. This technique makes it possible to achieve an active phased-array antenna system that offers high C/IM and high power efficiency, which will ease the heat dissipation problem anticipated for future communication satellites.

Acknowledgment

The authors would like to thank Dr. H. Mizuno, NTT Network Innovation Laboratories (now DoCoMo Inc.), Yokosuka, Japan, for his support and encouragement. The authors would also thank H. Okazaki, NTT Electronics, Machida, Japan, Y. Nakasuga, NTT Network Innovation Laboratories, Yokosuka, Japan, Y. Imaizumi, NTT Network Innovation Laboratories, F. Kira, NTT Network Innovation Laboratories, Y. Suzuki, NTT

Network Innovation Laboratories, S. Murakoshi, NTT Network Innovation Laboratories, and N. Sakamoto, NTT Advanced Technology, Yokosuka, Japan, for their valuable support.

REFERENCES

[1] T. Ohira, K. Ueno, K. Horikawa, and H. Ogawa, "Onboard active phased array techniques for high-performance communication satellites," in *Proc. IEICE MWE'97*, pp. 339–345.

[2] S. Torrents, J. Baucells, and J. Martinez, "An internally tuned Ku-band monolithic predistortion linearizer," in *Proc. 26th Eur. Microwave Conf.*, 1996, pp. 204–207.

[3] S. Narahashi and T. Nojima, "Non-linear distortion compensation techniques of power amplifiers for mobile communication systems," in *Proc. IEICE MWE'97*, pp. 87–92.

[4] T. Kaho, H. Okazaki, K. Horikawa, K. Araki, and T. Ohira, "Improvement technique in the C/I of a high-power amplifier array using intermodulation distortion controllers," in *Proc. RAWCON'99*, pp. 183–186.

[5] T. Kaho, H. Okazaki, Y. Nakasuga, K. Araki, and K. Horikawa, "Intermodulation distortion control technique for an onboard high-power amplifier array," in *Proc. AIAA–ICSSC*, vol. 144, 2001.

[6] T. Kaho, Y. Nakasuga, H. Okazaki, K. Araki, and K. Horikawa, "A distortion control technique for achieving high power efficiency in an HPA array," *IEEE Trans. Microwave Theory Tech.*, vol. 50, pp. 2505–2512, Nov. 2002.

[7] K. Horikawa and H. Ogawa, "Even-order distortion enveloping method to linearizer saturated high power amplifiers," in *Proc. IEEE MTT-S Int. Microwave Symp. Dig.*, 1997, pp. 79–82.

[8] T. Kaho, H. Okazaki, and T. Ohira, "A GaAs monolithic intermodulation controller for active phased array systems," in *Proc. Asia–Pacific Microwave Conf.*, 1998, pp. 603–606.

Takana Kaho was born in Sapporo, Japan, in 1971. She received the B.S. and M.S. degrees in physics from the Tokyo Metropolitan University, Tokyo, Japan, in 1994 and 1996, respectively.

In 1996, she joined NTT Wireless Communication System Laboratories (now NTT Network Innovation Laboratories), NTT Corporation, Yokosuka, Japan, where she has been engaged in research of satellite on-board amplifier.

Ms. Kaho is a member of the Institute of Electronics, Information and Communication Engineers (IEICE), Japan. She was the recipient of the 1998 Japan Microwave Prize presented at the Asia–Pacific Microwave Conference.

Tadao Nakagawa (M'91) received the B.E. and M.E. degrees in material physics and the Dr.Eng. degree in communication engineering from Osaka University, Osaka, Japan, in 1986, 1988, and 1997, respectively.

In 1988, he joined the NTT Radio Communication Systems Laboratories, Yokosuka, Japan, where he was engaged in research and development of MMICs and microwave synthesizers. From 1997 to 1999, he was an Associate Manager with the STE Telecommunication Engineering Company Ltd., where he served as a Technical Consultant on wireless communications to the Seiko Epson Corporation, Nagano, Japan. Since 1999, he has been a Senior Research Engineer with the NTT Network Innovation Laboratories, Yokosuka, Japan, where he is currently involved in the design of millimeter-wave transceivers and multiband transceivers.

Dr. Nakagawa is a member of the Institute of Electronics, Information and Communication Engineers (IEICE), Japan. He was the recipient of the 1995 Young Engineer Award presented by the IEICE.

Katsuhiko Araki received the B.E. and M.E. degrees from the Tokyo Institute of Technology, Tokyo, Japan, in 1979 and 1981, respectively.

In 1981, he joined the NTT Electrical Communications Laboratories, Yokosuka, Japan, where he was engaged in research on GaAs monolithic microwave circuits and the development of communication satellite on-board transponders. He is currently a Senior Research Engineer, Supervisor with NTT Network Innovation Laboratories, Yokosuka, Japan.

Mr. Araki is a member of the American Institute of Aeronautics and Astronautics (AIAA) and the Institute of Electronics, Information and Communication Engineers (IEICE), Japan. He was the recipient of the 1988 IEEE Sinohara Prize.

Kohji Horikawa (M'93) received the B.S. degree in electrical engineering from the Tokyo Institute of Technology, Tokyo, Japan, in 1984.

In 1984, he joined the Yokosuka Electrical Communication Laboratories, NTT Research and Development Bureau, where he was engaged in research and development of satellite on-board transponders. From 1993 to 1997, he was involved with research on optical/microwave interaction systems and photonic beam-forming networks for microwave active phased-array antennas. He is currently an Executive Engineer with the Radio Network Development Department, NTT DoCoMo Inc., Yokosuka, Japan.

Mr. Horikawa is a member of the Institute of Electronics, Information and Communication Engineers (IEICE), Japan.